Calf Spleen Purine Nucleoside Phosphorylase Complexed with Substrates and Substrate Analogues[†,‡]

Chen Mao,[§,||] William J. Cook,[⊥] Min Zhou,[§] Alexander A. Federov,[#] Steven C. Almo,[#] and Steven E. Ealick*[,§]

Section of Biochemistry, Cell and Molecular Biology, Cornell University, Ithaca, New York 14853, Department of Pathology, University of Alabama at Birmingham, Birmingham, Alabama 35294, and Department of Biochemistry, Albert Einstein College of Medicine, Bronx, New York 10461

Received September 26, 1997; Revised Manuscript Received March 2, 1998

ABSTRACT: Purine nucleoside phosphorylase (PNP) is a key enzyme in the purine salvage pathway, which provides an alternative to the de novo pathway for the biosynthesis of purine nucleotides. PNP catalyzes the reversible phosphorolysis of 2′-deoxypurine ribonucleosides to the free bases and 2-deoxyribose 1-phosphate. Absence of PNP activity in humans is associated with specific T-cell immune suppression. Its key role in these two processes has made PNP an important drug design target. We have investigated the structural details of the PNP-catalyzed reaction by determining the structures of bovine PNP complexes with various substrates and substrate analogues. The preparation of phosphate-free crystals of PNP has allowed us to analyze several novel complexes, including the ternary complex of PNP, purine base, and ribose 1-phosphate and of the completely unbound PNP. These results provide an atomic view for the catalytic mechanism for PNP proposed by M. D. Erion et al. [(1997) *Biochemistry 36*, 11735−11748], in which an oxocarbenium intermediate is stabilized by phosphate and the negative charge on the purine base is stabilized by active site residues. The bovine PNP structure reveals several new details of substrate and inhibitor binding, including two phosphate-induced conformational changes involving residues 33−36 and 56−69 and a previously undetected role for His64 in phosphate binding. In addition, a well-ordered water molecule is found in the PNP active site when purine base or nucleoside is also present. In contrast to human PNP, only one phosphate binding site was observed. Although binary complexes were observed for nucleoside, purine base, or phosphate, ribose 1-phosphate binding occurs only in the presence of purine base.

Purine nucleoside phosphorylase (EC 2.4.2.1, PNP) catalyzes the reversible phosphorolysis of ribonucleosides and 2′-deoxyribonucleosides to 2-deoxyribose 1-phosphate and the free purine bases. The reaction proceeds with inversion at C1′ as follows:

$$\beta\text{-nucleoside} + P_i \leftrightarrow \text{base} + \alpha\text{-ribose 1-phosphate}$$

PNPs are widely distributed in nature and have been identified and studied in various tissues (*2*). PNP is a key enzyme in the salvage pathway, which allows cells to utilize preformed bases and nucleosides to synthesize nucleotides. The salvage enzymes involved in the process allow circumvention of the respective de novo pathways when precursors are provided. In addition to its role in purine nucleotide metabolism, absence of PNP activity in humans has been associated with specific T-cell immune suppression, while B-cell function remains unaffected (*3*). For these reasons, PNP has been recognized as an important target for drug design.

Only three structures from the mammalian PNP family are known: (1) human erythrocytic PNP refined at 2.8 Å resolution (*4*), which provided structural details of the interactions in the active site and initiated structure-based drug design of PNP inhibitors, (2) a bovine PNP−inhibitor complex refined at 2.9 Å resolution (*5*), and (3) a bovine PNP−hypoxanthine complex refined at 2.15 Å resolution (*6*). Both bovine and human erythrocyte PNP have trimeric structures with three identical subunits of about 31 kDa. The sequence of bovine PNP is 86% identical to that of human erythrocyte PNP, and all residues of the active site are conserved. Most of the substitutions, except for residue 29 (Ile to Val), are on the surface of the enzyme or at the interface between subunits.

Crystals of human erythrocytic PNP were grown from high concentrations of ammonium sulfate, and the phosphate binding site was occupied by a sulfate ion. Consequently, the structures of the substrate-free and the ribose 1-phosphate complex could not be obtained with the human PNP crystals. This prevented exploration of the role of phosphate binding and its impact on other binding subsites. Furthermore, the

[†] This work was supported by Grants GM48874, RR01646, and CA67763 from the National Institutes of Health, the W. M. Keck Foundation, and the Lucille P. Markey Charitable Trust.

[‡] The Brookhaven Protein Data Bank codes for the structures reported herein are as follows: native PNP, 1PBN; PNP−phosphate, 1a9o; PNP−9-deazainosine−phosphate, 1a9p; PNP−inosine, 1a9q; PNP−inosine−sulfate, 1a9s; PNP−9-deazahypoxanthine−ribose 1-phosphate, 1a9t; and PNP−hypoxanthine, 1a9r.

* Corresponding author. E-mail: see3@cornell.edu.

[§] Cornell University.

[||] Present address: Hughes Institute, Roseville, MN 55112.

[⊥] University of Alabama at Birmingham.

[#] Albert Einstein College of Medicine.

S0006-2960(97)02391-X CCC: $15.00
Published on Web 04/29/1998

original human PNP crystals only diffracted to 2.8 Å resolution, and the structural analyses of most of the complexes were performed at 3.0−3.2 Å resolution, although the bovine PNP−hypoxanthine complex diffracted to a considerably higher resolution. Finally, the human PNP crystals were grown under acidic conditions (pH 5.4) far below the pH for optimum activity.

We have now grown crystals of bovine PNP from PEG 400 at pH 7.4−8.2, which is near the pH for optimal activity, and the structure has been determined and refined at 2.0 Å resolution. In addition, phosphate-free crystals have been obtained, and structures of various purine and purine nucleoside complexes, both with and without phosphate or ribose 1-phosphate, have been analyzed. These high-resolution structures of complexes with substrates and analogues provide information about the structural details of the catalytic mechanism, as well as new information about specific atomic interactions important for structure-based drug design. The crystal structure data suggest that, in the phosphorolytic direction, phosphate and inosine can bind PNP in either order but ribose 1-phosphate must be released before hypoxanthine. In the synthetic direction, however, ribose 1-phosphate can bind the enzyme only when hypoxanthine is present. The size and shape of the active site cavity change significantly upon phosphate binding. This observation may help explain the dependence of K_i on phosphate concentration for many competitive PNP inhibitors (*7*). This work also provides a framework for addressing some fundamental features of catalysis, including (1) the effect of substrate binding on enzyme structure, (2) the possible role of water in the PNP-catalyzed reaction, (3) further clarification of the roles for active site residues, (4) the structural basis of enzyme activity and inhibition, and (5) the structure of the transition state.

MATERIALS AND METHODS

Protein Preparation. Bovine spleen PNP was purchased from Sigma. After dilution in 50 mM TEA at pH 7.5, the solution was desalted by passing it over a Sephadex G-25 column. The eluant was dialyzed in 10 mM HEPES buffer at pH 7.0, and the protein was concentrated to 30−40 mg/mL by a Centricon-10 concentrator.

Crystallization. Crystals of PNP were obtained by the hanging drop method. The precipitating agent was 31−35% PEG 400 in 100 mM HEPES or Tris buffer (pH 7.8−8.2) and 100 mM $MgCl_2$. The addition of 1% octyl β-D-glucopyranoside resulted in larger crystals. The crystals grew from precipitate after 2 days and took 3−6 weeks to reach their maximum size, 0.2−0.6 mm on an edge. The crystal morphology ranged from tetrahedral to a tetragonal pyramid to a simple trigonal thick plate. The best data usually came from tetrahedral crystals. The protein crystallized in space group $P2_13$ with a unit cell length of 94.2 Å. Crystals were prepared for data collection by transferring them to a stabilizing mother liquor consisting of 50% PEG 400 in 100 mM HEPES buffer at the growth pH.

Preparation of PNP−Ligand Complexes. The ligands used in the soaking experiments included inosine, guanosine, hypoxanthine, ribose 1-phosphate, 2′,3′-dideoxyinosine, and 3′-deoxyguanosine, which were purchased from Sigma Chemical Co.; acyclovir diphosphate, which was provided by J. Tuttle of Burroughs Wellcome Co.; 9-deazainosine, which was provided by B. Klein of Montefiore Medical Center; and 7-deazainosine and 9-deazahypoxanthine, which were provided by J. Montgomery of Southern Research Institute.

Crystals were soaked for various periods in 3 mL of a stabilizing mother liquor containing substrates with concentrations ranging from 1.2 to 10 mM. A soak of 1 or 2 h was sufficient for the substrate to diffuse into the crystal and bind the enzyme. The crystals were immediately mounted after soaking. For data collection, crystals were mounted in siliconized glass capillaries. Tables 2 and 3 summarize the soaking experiments. Ligands were usually weighed in powder form and transferred to 1.5 mL of 210 mM HEPES buffer, which was stirred until most of the ligand dissolved. The solution was then slowly added to 1.5 mL of PEG 400 and the mixture stirred for 30 min.

Removal of Phosphate. A Fisher R218 column was used for the purification of PEG 400 for phosphate and sulfate ion contaminants. Phosphate assays were carried out using a malachite green−molybdate assay. This method can detect phosphate concentrations as low as 10 μM. The measurement used for the analyses of the mother liquor and the soaking solutions was calibrated according to standard samples of sodium phosphate monobasic under the same buffer conditions of the mother liquor. The mother liquor, using the purified PEG 400 through a Fisher R218 column, had no detectable phosphate. The measurement was repeated several times for various batches of mother liquor (always 3 mL in volume), each of which typically had been used for just one crystal.

The phosphate concentration of the mother liquor or of the ligand soaking solutions is typically around 70 mM. The precipitant PEG 400 (Fisher Co.) is the major source of phosphate contamination. The phosphate-free and sulfate-free conditions were achieved by using purified PEG 400 as the precipitant, and the crystals were either transferred to, or grown in, Tris buffer.

Data Collection. Data were collected on a Xuong-Hamlin twin detector system (San Diego Multiwire Systems, San Diego, CA). Monochromatic CuKα X-rays (1.54184 Å) were provided by a Rigaku RU-200B rotating anode generator operating at 100 mA and 40 kV. The X-ray beam was reflected from a graphite crystal to produce monochromatic radiation and collimated by a 0.3 mm aperture pinhole collimator.

A PNP crystal measuring slightly more than 0.3 mm on each edge was used for native data collection. The detectors were symmetrically offset by 23° relative to the direct beam for the collection of the 2.4 Å resolution data and 35° for the collection of the 1.9 Å resolution data. The crystal-to-detector distances for the two chambers were 560 and 500 mm, respectively. The data were collected at room temperature using ω-scans consisting of 0.1° steps for a total of 50−60°. The intensity data were indexed, integrated, scaled, and merged using San Diego Multiwire software. R_{sym} for the native data is 5.2% at 2.2 Å and 7.7% at 1.9 Å. The data completeness at 2.0 Å resolution is 92%, and the number of unique reflections with an amplitude cutoff of $F_{obs} > 2.0\sigma$ is 17 289.

The data for the crystals that were soaked with various substrates and inhibitors were generally collected by using

Table 1: Summary of Refinement Statistics for Bovine Spleen PNP and Complexes with Substrates and Analogues[a]

	native	phosphate[b]	9-deazainosine−phosphate	inosine[c,d]	inosine−sulfate	9-deazahypoxanthine−ribose 1-phosphate	hypoxanthine[d]
soak conditions	Tris buffer (phosphate- and sulfate-free)	70 μM	4 mM 9-deazainosine and 4 mM phosphate	7.3 mM inosine	12.8 mM inosine and 12 mM sulfate	4 mM 9-deazahypoxanthine and 4 mM ribose 1-phosphate	1.2 mM hypoxanthine
resolution range (Å)	8.0−2.0	8.0−2.0	8.0−2.4	8.0−2.0	8.0−2.0	8.0−2.0	8.0−2.0
R factor (%)	20	20	19	20	18	19	19
number of reflections	14 137	17 289	10 457	15 990	15 060	14 891	14 482
completeness (%)	82	92	97	89	83	80	80
number of waters	43	35	25	55	52	56	55
average *B* factor (Å^2)	23	16	12	19	14	15	19
deviations from ideality							
bond lengths (Å)	0.006	0.007	0.007	0.006	0.006	0.006	0.006
bond angles (deg)	1.51	1.64	1.66	1.54	1.53	1.56	1.52
improper angles (deg)	1.18	1.24	1.17	1.11	1.12	1.17	1.11

[a] Amplitude cutoff was 2.0σ for all data sets. [b] Phosphate is normally present in the mother liquor at about 70 μM. The PEG 400 is the source of the trace phosphate. [c] Inosine soak results in an apparent hydrolysis by PNP; only hypoxanthine is seen in the active site. [d] Sulfate contaminant may come from the HEPES buffer, and it causes a 0.5−0.7 occupancy of sulfate in the phosphate binding site.

Table 2: Summary of Difference Fourier Results with Phosphate-Contaminated Crystals[a]

ligand	concentration[b] (mM)	soak time (days)	resolution (Å)	R_{sym} (%)	completeness (%)	summary of $F_{complex} - F_{native}$ maps
Na_2SO_4	5.3	3	2.2	9.7	91	no peak at the phosphate binding site
Na_2HAsO_4	4.1	5	3.0	10.0	98	large peak at the phosphate binding site
acyclovir diphosphate	4.0	7	2.2	8.5	92	acyclovir diphosphate
9-deazainosine	4.0	2	2.2	7.5	92	9-deazainosine
inosine and sulfate	10.0 and 10.0	21	2.2	10.7	91	inosine
inosine	4.0	2	3.0	11.5	98	hypoxanthine and ribose 1-phosphate
9-deazahypoxanthine and ribose 1-phosphate	4.0 and 4.0	9	2.5	11.0	98	9-deazahypoxanthine and ribose 1-phosphate
ribose 1-phosphate	4.0	1	2.5	11.0	98	no density for ribose 1-phosphate
hypoxanthine	4.0	6	3.0	12.7	77	hypoxanthine[c]
hypoxanthine and phosphate	1.2 and 1.0	0.04	3.0	10.0	98	hypoxanthine

[a] The difference Fourier maps were calculated using the data from the soaked crystal and the data from a native crystal in Tris buffer, which had no detectable phosphate contaminants. [b] Ligand concentrations are based on calculation. For an insoluble sample compound such as ribose 1-phosphate, the real concentration is a saturated one. [c] Although the electron density is noisier than the soak with hypoxanthine and 1.0 mM phosphate, the presence of hypoxanthine is certain.

twin detectors asymmetrically offset by 30 and −23°. Depending on the quality of the crystals and the soaking solution, the resolution of the data typically varied from 2.3 to 3.0 Å.

Structure Determination. The structure of bovine spleen PNP was solved by molecular replacement, using the programs AMORE (*8*) and XPLOR (*9*). The search model was the human PNP monomer, and the 40 nonconserved residues were replaced by Gly or Ala residues. The rotation searches gave peaks with high contrast at an expected orientation, assuming the PNP trimer uses the crystallographic 3-fold axis of space group $P2_13$. The translation search also gave a large signal. Following a rigid-body refinement, the initial *R* factor was 38% in the resolution range of 15−4 Å. The key residues in the active site (residues 84, 86, 88, 219, 210, 211, 159, 66, and 64) were changed to Ala or Gly and refitted after simulated annealing refinement. These residues were visible in the $2F_o - F_c$ map after the initial refinement. Residues 246−249 and the loop around His64 were completely rebuilt. Refinement was carried out by the simulated annealing algorithm in XPLOR with manual refitting after each cycle. The free *R* factor (*10*) was used for cross validation throughout the refinement. Water molecules were added to the model when density peaks were at least 4σ in $F_o - F_c$ maps and when they formed appropriate hydrogen bond contacts.

The 9-deazainosine and phosphate substrates were fit into the electron density of $F_o - F_c$ maps and refined by simulated annealing in XPLOR. The initial structure of 9-deazainosine was taken from the refined human PNP−9-deazainosine

Table 3: Summary of Difference Fourier Results with Phosphate-Free Crystals in HEPES or Tris Buffer[a]

ligand	concentration[b] (mM)	resolution (Å)	R_{sym} (%)	completeness (%)	summary of $F_{complex} - F_{native}$ maps
inosine	7.3	1.9	9.3	86	hypoxanthine
guanosine	3.0	1.9	7.7	89	guanine
3′-deoxyguanosine	3.0	1.9	10.0	86	guanine
2′,3′-deoxyguanosine	3.0	3.0	12.5	98	guanine
7-deazainosine	4.4	2.5	12.0	97	7-deazainosine
formycin B	1.2	3.0	13.0	95	formycin B[c]
hypoxanthine	1.2	1.9	6.9	76	hypoxanthine
ribose 1-phosphate	1.5	2.2	9.1	88	phosphate[d]

[a] The difference Fourier maps were calculated using the data from the soaked crystal and the data from a native crystal in HEPES buffer, which had no detectable phosphate contaminants. The soak time was 1 h for all experiments except that with ribose 1-phosphate, in which case it was 8 days. [b] Ligand concentrations are based on calculation. For an insoluble compound such as ribose 1-phosphate, the real concentration is a saturated one. [c] Formycin B soaking reproducibly resulted in nonisomorphic data, but the presence of formycin B is certain. [d] Phosphate presumably derived from the decomposition of ribose 1-phosphate.

complex at 3.0 Å resolution. Stereochemical parameter files defined by Engh and Huber (*11*) were used for protein refinement parameters. The parameter and topology files were generated for the nucleosides using the toph11.dna and param11.dna files provided in XPLOR, modified to reflect experimentally derived constants for 9-deazainosine.

The other complex structures were determined by starting with the refined models of phosphate and 9-deazainosine complexes. One round of simulated annealing refinement in XPLOR (*10*) against the data of the complex decreased the *R* factor well below 30%. By inspection of the $F_o - F_c$ maps at the 4σ level, the $2F_o - F_c$ maps at the 1σ level, and the F_o(complex) $- F_o$(native) maps, substrates and water molecules were fit into density conservatively. The F_o-(complex) $- F_o$(native) maps were calculated using phases from refined structures, initially without the three loop regions that were considered the most flexible (residues 31−36, 56−66, and 246−266).

The free *R* factor was used as the major index of the refinement progress. The calculated weight on the diffraction data was lowered by 2−3 times to achieve the lowest R_{free} value. The initial geometry largely relied on the difference Fourier maps and the $F_o - F_c$ map phased by the refined structure at 2.0 Å. Since the high-resolution electron density provided very good initial coordinates, user-defined parameters of bond angle and bond length were employed in addition to the available force constants, bond angle, and bond length initially modified from parameter files provided by XPLOR. The water molecule positions were fixed during simulated annealing refinement. All charges on residues or substrate were set to zero to avoid the bias of strong charge interactions. The final geometry largely depends on electron density, because the geometry of substrates and/or analogues such as ribose 1-phosphate could be very different in enzyme or in solution.

Refinement. The PNP complex structures were refined at 2.0−2.4 Å resolution (Table 1). The free *R* factor was used to monitor every cycle of the refinement, and the weight on the crystallographic term of refinement calculated in XPLOR was divided by 2.5 to optimize R_{free}. Water molecule positions were fixed during the simulated annealing refinement. The various ligand molecules were initially placed according to the peaks in the difference Fourier maps and then refined.

RESULTS AND DISCUSSION

Structure of Unliganded Bovine Spleen PNP. In the previously reported structure determination of human PNP, the phosphate binding site was occupied by sulfate (*4*). To study unliganded PNP, and the structures of various complexes in the absence of phosphate, we crystallized phoshate-free bovine PNP. These efforts were complicated by phosphate contaminants in PEG 400, which was used as the precipitating agent, and sulfate contaminants in the HEPES buffer. These contaminants were discovered when the initial crystals of bovine PNP failed to show the expected difference Fourier peaks after soaking in either 1 mM phosphate or 5.3 mM sulfate. Subsequent analysis of the mother liquor showed that the phosphate concentration was 70 μM. These problems were not encounterd by Koellner et al. (*6*) in their crystallographic analysis of the bovine PNP−hypoxanthine complex.

Evidence that phosphate fully binds the enzyme, even at a concentration as low as 70 μM, became convincing after refinement of the initial bovine PNP structure at high resolution. The $F_o - F_c$ map calculated at 2.0 Å resolution with the refined protein structure (no phosphate ion in the model) showed a single tetrahedral molecule in the expected phosphate binding site. A soak in arsenate also gave one large peak at this position because of the increased electron density relative to phosphate. Furthermore, soaking with acyclovir diphosphate, which is a potent PNP inhibitor (*12*), showed the complete density of the molecule in difference Fourier maps, except for the terminal phosphate group, indicating that the presumed unliganded PNP structure was not really phosphate-free.

Large crystals were eventually grown from phosphate-free PEG 400 and transferred to Tris buffer to remove the sulfate contaminant derived from the HEPES buffer. These crystals were shown to be phosphate-free by crystallographic refinement and by analyzing difference Fourier maps between the phosphate-free crystals and crystals soaked with phosphate or sulfate. These maps showed obvious peaks in the difference Fourier maps.

The overall structure of bovine PNP is similar to that of human PNP (*4*) and essentially the same as the earlier structures of bovine PNP complexes reported by Bzowska et al. (*5*) and Koellner et al. (*6*). The enzyme is a trimer with identical subunits and one active site per subunit (Figure 1). Each subunit has an α/β structure with a central eight-strand mixed sheet and a smaller five-strand sheet. The statistics of the refined structures of unliganded bovine PNP and various substrate complexes are summarized in Table 1. On the basis of the sequence alignment, the differences between bovine PNP and human erythrocytic PNP amino

FIGURE 1: Bovine PNP trimer. Residues that differ from human PNP are red. Coordinates for 9-deazainosine and phosphate (yellow) are from the bovine PNP complex [Figures 1, 2, 4, 5, and 7 created with RIBBONS (*24*)].

acid sequences are illustrated in Figure 1. Nearly all of these difference are located on the surface of the protein and have little effect on the overall structure. The only buried substitution, Ile to Val at position 29, is conservative and does not directly affect the active site.

The α-carbon atoms in the native structure of bovine PNP can be superimposed with corresponding atoms in human PNP with a root-mean-square deviation of 2.0 Å, using the superposition method of Kabsch (*13*). However, this relatively large deviation is primarily due to large differences in poorly defined loops and the two termini. The residues that differ the most are 1 and 2, 32−37, 58−66, 180−184, 250−264, and 284−289. When these residues are excluded, the root-mean-square deviation is only 0.4 Å. These differences may result primarily from random disorder because comparisons of complex structures of bovine and human PNP reveal much smaller differences. In these structures, the binding of a substrate or analogue increases the percentage of secondary structure and stabilizes the loops, making them much better defined in the electron density maps. For example, comparison of the α-carbon atoms in bovine PNP−9-deazainosine−phosphate (see below) with those in human PNP−guanine−sulfate gives a root-mean-square deviation of only 1.3 Å for all atoms. Even in this case, however, the same loops contribute most of the large differences. The sole exception is the loop containing residues 32−37, which is quite similar in these two structures.

Examination of the average *B* factors in the bovine PNP structures (Table 1) confirms the relatively high mobility of these loop residues. The highest *B* factors in the molecule occur in the loop containing residues 244−266, although *B* factors of these residues tend to be lower in the complex structures. This reflects the increased secondary structure in this region (from coil to helix) upon binding of purine substrates or analogues (Figure 2). Except for the loop regions involving residues 244−266, which are highly disordered in unliganded PNP, all the refined structures have torsion angles in the allowed regions. One exception is Thr221, which has nonideal torsion angles in almost all of the structures.

Phosphate Binding in Complexes with Phosphate, Sulfate, and Arsenate. Analysis of the PNP crystals containing phosphate, sulfate, or arsenate confirmed the participation of the side chains of Ser33, Arg84, His86, and Ser220 and the main chain N atoms of Ser33 and Ala116 in the binding site for phosphate, as was the case for human PNP (*4*). However, when those structures were compared to unliganded PNP, large conformational changes of residues in the phosphate binding site (33−36 and 56−69) were also visible (Figure 2). Figures 3 and 4 show details of the phosphate binding site. As is the case for human PNP, O3 of phosphate forms hydrogen bonds to the main chain N atoms of both Ser33 and Ala116, phosphate atom O1 forms a hydrogen bond with OG of Ser33, and phosphate atom O4 forms hydrogen bonds with an active site water molecule and Ser220.

The changes in the loop of residues 33−36 are small; however, the loop involving residues 56−69 shows substantial differences from the human PNP model (Figure 2). The new positions of these loops are consistent in all the difference Fourier maps for PNP complexes containing phosphate. Unlike the analysis of the structure of human PNP, which showed only two positively charged residues (Arg84 and His86) involved in phosphate binding, this analysis confirms the participation of His64 (Figures 3 and 4). The positions of Arg84 and His86 move very little between phosphate-bound and phosphate-free enzyme. However, His64 moves considerably as a result of the conformational change that occurs when the phosphate site is occupied. Both conformational changes were also observed when the phosphate binding site was occupied by ribose 1-phosphate, acyclovir diphosphate, sulfate, or arsenate.

The changes in these two regions (residues 32−36 and 56−69) are associated only with phosphate binding but show variation depending on the phosphate concentration. In the absence of phosphate, these residues assume one conformation. In phosphate at high concentrations (>1 mM), these loops are well-ordered and form close contacts between side chains and phosphate ion, especially Ser33 and His64, resulting in a different conformation. At low phosphate concentrations (unpublished data), the loops appear at an intermediate position and the electron density maps cannot easily be interpreted as a simple average of the two conformations. It is possible that this effect can be explained by communication between subunits and that the loops in the phosphate binding site are different depending on whether all three active sites are occupied. The conformational changes in the phosphate binding site appear to be independent of purine or purine nucleoside binding.

The crystal structure of human erythrocytic PNP suggested the possibility of a sulfate ion at the entrance of the active site, providing some evidence for a second phosphate binding site (*4*). A recent study of bovine PNP activity as a function of phosphate concentration also supported a model for two separate phosphate binding sites in the enzyme (*14*). However, the current high-resolution structures with and without phosphate provide no evidence for a second binding site.

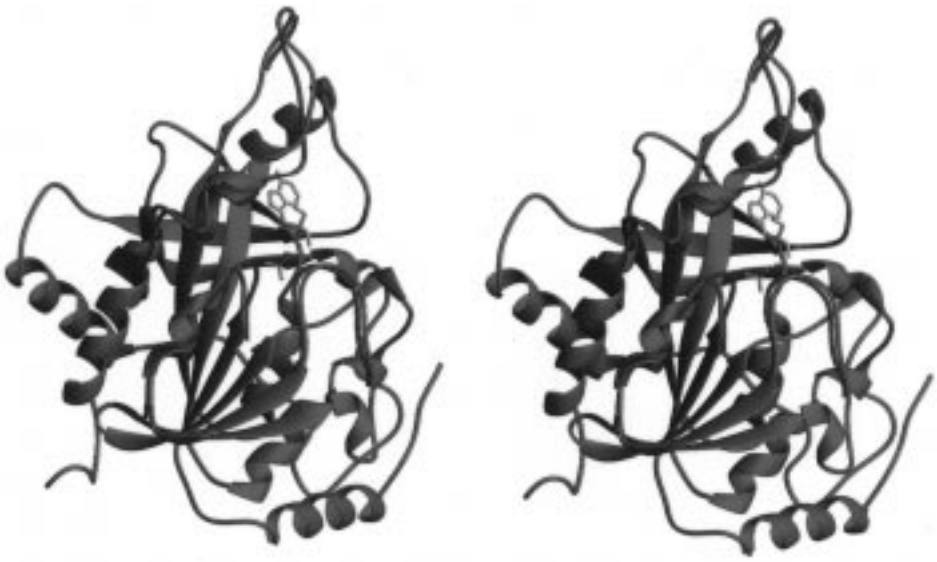

FIGURE 2: Stereoview of bovine PNP monomer (cyan) with superimposed loops (red) and substrate molecules (yellow) from the PNP−phosphate−9-deazainosine complex.

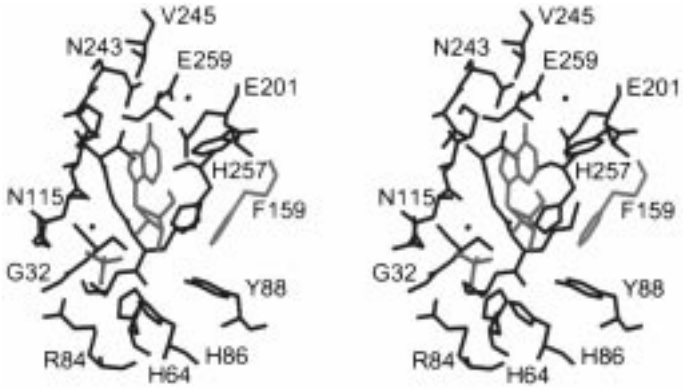

FIGURE 3: Stereoview of the active site in bovine PNP complexed with inosine and sulfate. Residues 32, 33, 64, 84, 86, 88, 115−118, 200, 201, 217−220, 242, 243, 245, 257, and 259 are from one subunit (blue), and residue 159 from an adjacent subunit is magenta. Two water molecules are also included. Models of inosine and sulfate are red. The β-strand at the back of the active site (residues 217−220) is not labeled. [Figures 3 and 6 created with CHAIN (*25*)].

Nucleoside Binding in the Presence of Phosphate in PNP Complexes with 9-Deazainosine−Phosphate and Inosine−Sulfate. Nucleoside binding in the presence of phosphate was explored by preparing the ternary complex of PNP, 9-deazainosine (a noncleavable substrate analogue), and phosphate. Soaking with 4 mM 9-deazainosine (Table 2) in the presence of phosphate demonstrated clear electron density for both phosphate and 9-deazainosine. The refined occupancies for both substrates are near 100%. The expected conformational change for residues 244−266, which position the purine binding residues, was also observed as were the conformational changes associated with phosphate binding. The hydrogen bonding pattern of 9-deazainosine is essentially the same as that of the human PNP−9-deazainosine complex, except that this model includes participation of His64 and two water molecules in the active site.

Phosphate-free bovine PNP crystals soaked with 10 mM inosine and 10 mM sulfate demonstrated both inosine and sulfate in the active site. Apparently, 10 mM sulfate inhibits the hydrolysis that is normally observed in the absence of phosphate. The resulting PNP−inosine−sulfate complex is similar to the PNP−9-deazainosine−phosphate complex. Together, the two ternary complexes described here provide an attractive model for the PNP−substrate complex which, because of the high catalytic activity of PNP crystals, cannot be observed directly.

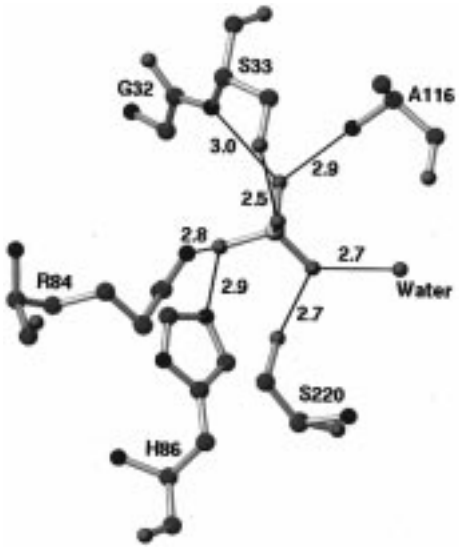

FIGURE 4: Detailed view of the hydrogen bonding scheme around the sulfate (phosphate) ion in the bovine PNP complex with inosine and sulfate. Atoms are coded as follows: carbon, green; nitrogen, blue; oxygen, red; and sulfur, yellow.

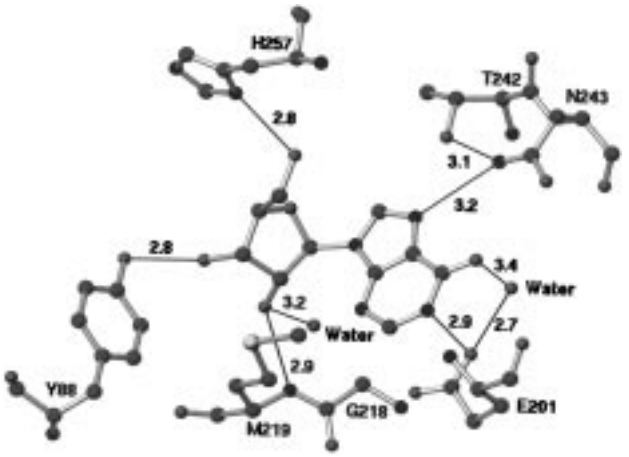

FIGURE 5: Detailed view of the hydrogen bonding scheme around inosine in the bovine PNP complex with inosine and sulfate. Same color scheme as that in Figure 4.

Interestingly, crystals of human PNP soaked with 4 mM inosine resulted in only hypoxanthine bound to the active site even though human PNP crystals are grown from 55−60% ammonium sulfate. It is possible that the differences in the rates of hydrolysis could be attributed to the differences in pH of the two kinds of PNP crystals or that some other reaction is taking place in the case of human PNP. In human PNP crystals, His64 is probably protonated (pH 5.2) and is away from the active site. In this case, the sugar ring can still be accessed by solvent and may be hydrolyzed more easily. In bovine PNP crystals (pH 8.0), His64 is probably unprotonated, resulting in a closed loop which may protect the substrate in the PNP−inosine−sulfate complex from hydrolysis.

Site-directed mutagenesis showed that both Asn243 and Glu201 are key residues for catalysis. Mutation of either of these residues to alanine greatly reduces the activity of PNP (*15*). An important difference between the structures of the 9-deazainosine and the inosine complexes is the conformation of the Asn243 side chain. In the inosine complex, the Asn243 side chain donates a hydrogen bond from ND2 to purine N7 and the O6 is linked to Glu201 through a bridging water molecule (Figures 3 and 5). The role of Asn243 as a hydrogen bond donor is consistent with the catalytic mechanism proposed by Erion et al. (*1*). However, in the case of 9-deazainosine, the N7 of purine is protonated and consequently the hydrogen bonding scheme is different. In this case, Asn243 OD1 accepts a hydrogen bond from purine N7, Asn243 ND2 donates a hydrogen bond to purine O6, and the bridging water molecule to Glu201 is not observed.

In addition to the two hydrogen bonds between O2′ and O3′ of the ribose and phosphate oxygen atoms O1 and O4, there are eight other hydrogen bonds involving the four phosphate oxygen atoms. Atom O1 of the phosphate interacts with both Ser33 and the 3′-hydroxyl group, while O2 interacts with Ser220, the 2′-hydroxyl group, and a highly ordered water molecule. This water molecule, which also forms hydrogen bonds with OH of Tyr192 from the core and the carbonyl group of Ala116, is present in complexes both with and without nucleoside. The phosphate O2 atom forms three hydrogen bonds with basic residues His64, Arg84, and His86. The orientation of His86 suggests that it is likely to form a strong hydrogen bond with O2 (2.9 Å) and possibly an electrostatic interaction (3.3 Å) with O1 of phosphate. On the other hand, Ser33 and the 3′-hydroxyl are clearly hydrogen-bonded to phosphate through O1, which is the oxygen atom expected to attack C1′ during catalysis. This suggests that Ser33 and the 3′-hydroxyl are necessary to correctly orient the key atoms of the phosphate and sugar.

This hydrogen bonding pattern in the PNP−nucleoside complexes is similar to what has been described in G proteins (*16*, *17*). Asn265 in the G protein occupies a position that corresponds to Asn243, and atom ND2 forms a hydrogen bond to N7 of the guanine base. A second hydrogen bond from ND2 is formed with a carbonyl oxygen from Ser40, while in PNP, it is the Thr242 side chain. Although this places atom OD1 of Asn265 relatively close to O6 (3.2 Å), its position is stabilized by three hydrogen bond interactions with the main chain N atom of Lys266 as well as OG1 from Thr320 and the main chain N of Ala322 from an adjacent strand. These stabilizing interactions are not present in bovine PNP. Asp268 in the G protein occupies a position similar to Glu201, but the close contact between OD1 and C2 in the base is not present, because the amino group at C2 forms a hydrogen bond with the carboxylate oxygen. The function of the two corresponding residues in the G protein (Asn265 and Asp268) was interpreted as alignment of the base plane. Although they probably serve a similar purpose in PNP, it is likely Asn243 has the additional function of donating a hydrogen bond to stabilize the negative charge that accumulates on the purine base during glycosidic bond cleavage (*1*). In the *Escherichia coli* PNP structure (*18*), Asp204 is in the same position as Asn243 and probably is required for catalysis.

Nucleoside Binding in the Absence of Phosphate in PNP Complexes with 7-Deazainosine and Formycin B. Native crystals treated with inosine, guanosine, and other substrates in the absence of phosphate show only the purine base in the final difference electron density maps (Tables 2 and 3). Kline and Schramm (*19*) reported a similar result in solution studies and demonstrated that PNP catalyzed a phosphate-independent hydrolysis. To further explore nucleoside binding in the absence of phosphate, we selected two purine nucleoside analogues that would be resistant to hydrolysis. Crystals treated with 7-deazainosine showed clear electron density for the intact nucleoside. Furthermore, crystals soaked with formycin B (a noncleavable inosine analogue) showed intact formycin B in the active site. Both inosine analogues induced the conformational change in residues 244−266 previously observed for purines and purine nucleosides. However, no conformational changes were observed in the phosphate binding site. The overall binding geometry and nucleoside conformation were similar to those of the ternary complexes, suggesting that the nucleoside binding site is not strongly affected by the phosphate binding site.

Purine Binding in the Presence of Ribose 1-Phosphate in Complexes with Ribose 1-Phosphate−Hypoxanthine and Ribose 1-Phosphate−9-Deazahypoxanthine. When a phosphate-contaminated crystal is soaked in a 4 mM solution of inosine, the electron density map shows hypoxanthine and α-ribose 1-phosphate (Table 2). This demonstrates that PNP in the crystal is active and, under these conditions, binds ribose 1-phosphate in the presence of hypoxanthine. PNP crystals soaked with 4 mM ribose 1-phosphate and 4 mM 9-deazahypoxanthine also showed both substrates in the

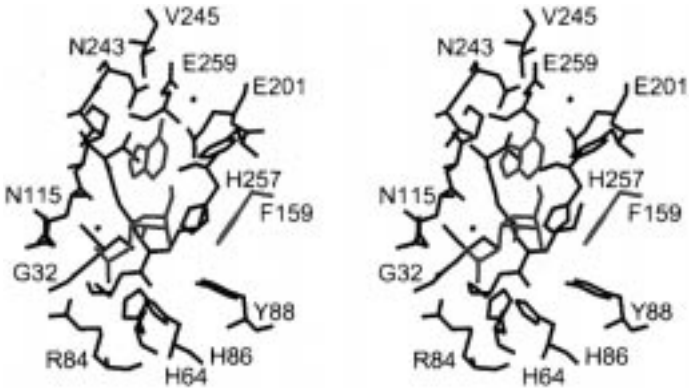

FIGURE 6: Stereoview of the active site in bovine PNP complexed with ribose 1-phosphate and 9-deazahypoxanthine. The orientation and residues are the same as those in Figure 3.

active site (Table 2 and Figure 6). Compared to that of native PNP, His257 moves closer to ribose 1-phosphate after the purine-induced conformational change in the loop containing residues 244−266. On the other hand, soaking a phosphate-contaminated or a phosphate-free native crystal in a 4 mM solution of ribose 1-phosphate produced no binding of ribose 1-phosphate to the enzyme (Tables 2 and 3). Instead, the trace amount of phosphate that is formed in the latter case from the decomposition of ribose 1-phosphate (<5%, according to the measured value) occupies the phosphate binding site. Because ribose 1-phosphate alone does not bind PNP, it may be that hypoxanthine increases the affinity of PNP for ribose 1-phosphate by creating new hydrogen bonds that result from the hypoxanthine-induced conformational change.

The structural details of the two PNP−purine−ribose 1-phosphate ternary complexes are essentially the same and serve as a model for the PNP−product complex following phosphorolysis. Furthermore, the structures of the PNP−product complex and the PNP−substrate complex are very similar. A structural comparison reveals that all active site residues involved in binding are in about the same position for both substrate and product (Figure 7). Table 4 lists the bond distances between the substrates and active site residues.

Purine Binding in the Absence of Phosphate in PNP−Hypoxanthine and PNP−Guanine. Purine base binding induces the expected conformational change in the loop containing resides 244−266 irrespective of the presence or absence of phosphate. Analyses of difference Fourier maps demonstrate that hypoxanthine binding in the absence of phosphate produces no significant changes in the phosphate binding site. These data together with the results described above suggest that the two types of conformational changes (i.e., purine-associated and phosphate-associated) are structurally independent.

Complexes of purine bases with PNP can also be prepared directly or indirectly by treating phosphate-free crystals with nucleosides. In solution, phosphate-free PNP catalyzes the hydrolysis of inosine to hypoxanthine and ribose (*19*). Our results suggest that crystalline PNP can also catalyze the hydrolysis of nucleosides (Table 2). Treatment of a phosphate-free crystal with inosine leads to a hypoxanthine-bound complex with no indication of ribose 1-phosphate or phosphate binding. This is clearly different from the results of the inosine soak in the presence of phosphate, which showed binding of hypoxanthine and ribose 1-phosphate.

Table 4: Hydrogen Bond Interactions in the Active Site of Bovine PNP

	residue	inosine−sulfate (Å)	9-deazahypoxanthine−ribose 1-phosphate (Å)	hypoxanthine−phosphate (Å)
base				
N1	Glu201 OE2	3.0	2.8	2.8
N7	Asn243 ND2	2.9	2.9	2.9
O6	water	3.4	3.0	3.1
sugar				
O2′	Met219 N	2.8	3.0	N/A[a]
O2′	phosphate O4	3.0		N/A
O3′	Tyr88 OH	2.8	3.0	N/A
O3′	phosphate O1	2.6		N/A
O5′	His257 ND1	2.8	3.0	N/A
O5′	Glu259 OE1	3.1	no bond	N/A
phosphate				
O1	Ser33 OG	2.6	3.0	no bond
O2	His64 NE2	3.1	no bond	no bond
O2	Arg84 NH1	2.8	3.0	2.7
O2	His86 NE2	2.9	2.9	no bond
O3	Ser33 N	3.1	3.1	no bond
O3	Ala116 N	2.8	2.9	3.0
O4	Ser220 OG	2.7	2.6	2.5
O4	water	2.7	2.7	no bond

[a] N/A means not applicable in the case of the hypoxanthine/phosphate complex with PNP.

Although inosine hydrolysis by crystalline PNP is consistent with the results of Kline and Schramm (*19*), one-third of the site's reactivity described in that paper could not be confirmed for either the inosine soak or the hypoxanthine soak (Table 2) because, under the conditions used here, the difference Fourier maps showed nearly full occupancy of hypoxanthine.

The water molecule that forms a hydrogen bond to Glu201 in nucleosides also forms a hydrogen bond with O6, as seen in the hypoxanthine complex structure. This water molecule, which was postulated by Erion et al. (*1*), could play a role in the reaction mechanism. In the nucleoside complex, the hydrogen bond is weaker than that for purine base alone. This is due in part to the positioning of the purine bases for the two cases. For hypoxanthine, the base is deeper in the active site and close to the water molecule, while in the

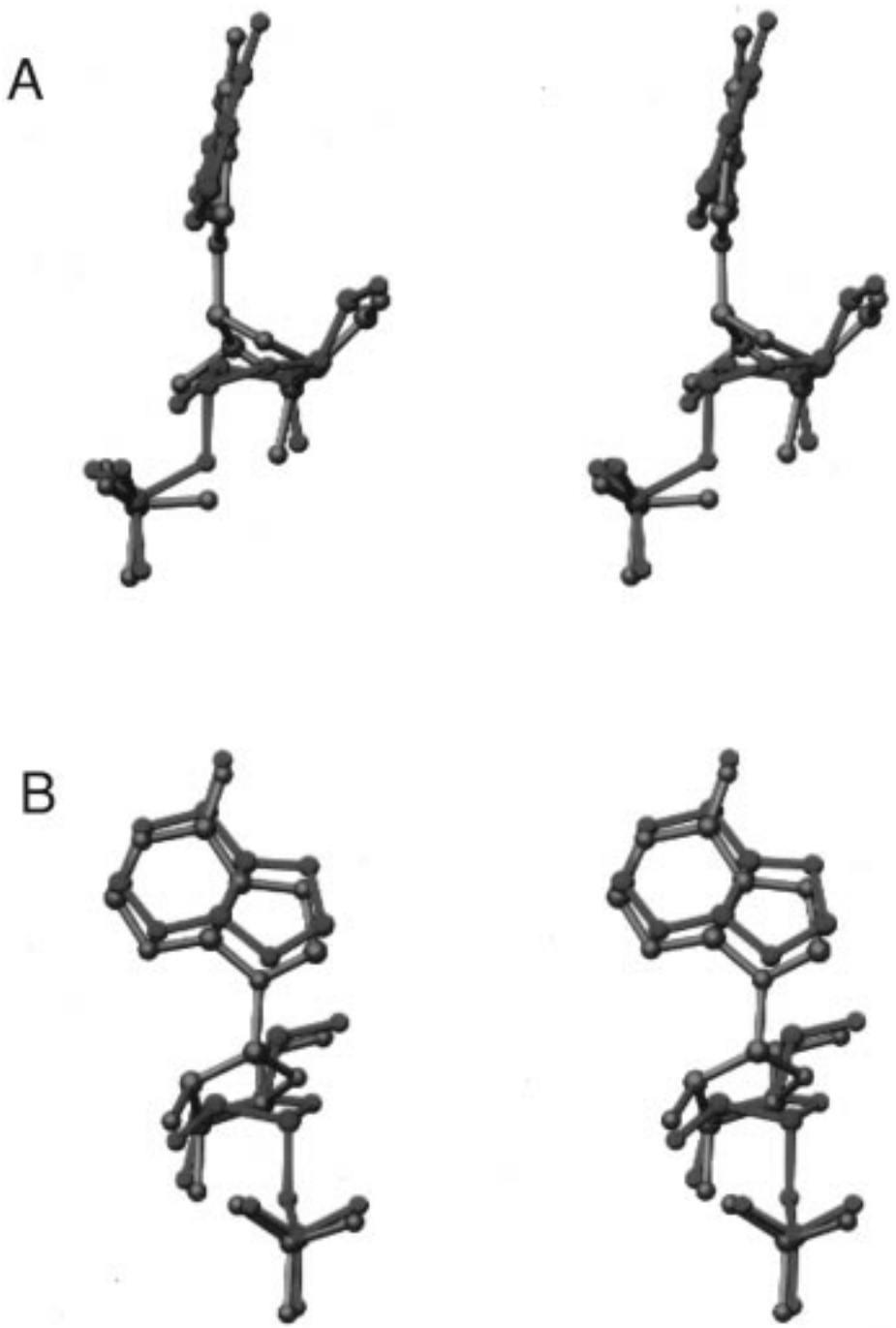

FIGURE 7: Stereoviews of the superposition of the reactants and products in the active site. Coordinates for inosine and sulfate (orange) and 9-deazahypoxanthine−ribose 1-phosphate (green) are from the corresponding complexes with bovine PNP. The views in panels A and B differ by a 90° rotation.

nucleoside complex, the base shifts toward the ribosyl group and away from the water molecule. It should also be noted that adenosine and adenine, which are very slow substrates for mammalian PNP, have amino groups at the 6-position. Although the binding geometry is the same as that for 6-oxopurines, the water molecule cannot form the same hydrogen bonds which could further explain the extremely slow rate of catalysis. In addition to the hydrophilic interactions with Asn243 and Glu201, there are a number of hydrophobic interactions surrounding the purine base, including Phe200, Val245, Val217, Met219, residues 116−119 of the β5 strand (AAGG), and Phe159 from a neighboring subunit (Figure 3).

Purine Binding in the Presence of Phosphate in Complexes with Phosphate−Hypoxanthine and Acyclovir Diphosphate. In crystalline PNP, purine bases can bind to the active site whether phosphate is present, even though the resulting purine−phosphate complex is unproductive for catalysis. The structure of the hypoxanthine−phosphate complex is essentially the same as the structure of human PNP complexed with sulfate and purine (*4*). However, Lys244, which was poorly defined in the human PNP structure, clearly does not contribute to purine binding in the bovine PNP structure. The specificity for 6-oxopurines is provided by hydrogen bonds from N1 of the purine base to Glu201 and from N7 to Asn243. Additional hydrogen bonds are provided by a

water molecule that bridges Glu201 and O6 of the purine base. Acyclovir diphosphate is a potent PNP inhibitor with a K_i of 8 nM when assayed at 1 mM phosphate. Its high affinity for PNP results from simultaneous occupation of both the purine and phosphate binding sites by groups that are covalently linked. The purine base and terminal phosphate are linked by a seven-atom spacer, and the position of the purine base resembles that of the hypoxanthine complex. Because of the long spacer, the geometry for the PNP−acyclovir diphosphate complex is most similar to that of the PNP−hypoxanthine−phosphate complex.

A disordered region (residues 244−266) becomes ordered and extends helix α7 by a little more than one turn at its N-terminal end (residues 258−266) when the base site is occupied. The conformational change is independent of phosphate binding as shown by the structures reported here. However, in the presence of high phosphate or sulfate, hypoxanthine occupancy is reduced while nucleoside occupancy is unaffected. Although the conditions and environment in crystalline PNP may be atypical, it is interesting to speculate that the negative charge of phosphate may disfavor the nonproductive addition of purine base.

Structure−Activity Relationships. The interactions between PNP and the sugar ring in the complex structures are primarily hydrophobic. However, there are also hydrogen bond interactions with three residues: Met219, Tyr88, and His257. In particular, atoms O2′ and O3′ form hydrogen bonds to Met219 and Tyr88, respectively, as well as important hydrogen bond interactions to the phosphate ion oxygen atoms, while His257 forms a hydrogen bond to O5′. This hydrogen bonding pattern can be use to explain the importance of sugar hydroxyls in the reaction mechanism. Both ribonucleosides and 2′-deoxyribonucleosides are good substrates; however, 3′-deoxyinosine is a very poor substrate (*20*). In the absence of a 2′-hydroxyl group, hydrogen bonding occurs only with O3′. In the absence of a 3′-hydroxyl group, the sugar conformation is distorted to optimize the hydrogen bonds to O2′, resulting in poor geometry for catalysis. Interestingly, 2′,3′-dideoxyinosine is a better substrate than 3′-deoxyinosine but poorer than 2′-deoxy substrates, probably because the lack of both hydroxyl groups allows the formation of a weaker but undistorted complex. This hypothesis has been confirmed by crystallographic studies of human PNP complexed with 3′-deoxyinosine and 2′,3′-dideoxyinosine (unpublished results). The hydrogen bonds between nucleoside hydroxyl groups and phosphate suggest that the binding of either nucleoside or phosphate will enhance binding of the other substrate. In the crystallographic analyses, soaking experiments showed that sulfate occupancy increased in the presence of 7-deazainosine even though the sulfate concentration was held constant.

In addition, the structures reported here may help to explain the dependence of K_i on phosphate concentration observed for many PNP inhibitors (*7*). Although in some cases this effect may be due mostly to direct competition of phosphate and inhibitor for the phosphate binding site (e.g., acyclovir diphosphate), in other cases the reason is not so obvious. However, since phosphate binding results in two conformational changes, it may be that the resulting rearrangement of residues decreases the binding affinity for a variety of nucleoside analogues.

Transition State Model. The crystallographic data provide evidence for the structures along various points of the reaction coordinate for the PNP-catalyzed reaction. Of particular interest are the structures of the enzyme−substrate and enzyme−product complexes. Figure 7 shows the active site of PNP with both reactants and products superimposed. In phosphorolysis, the active site orients the nucleoside so that the attacking phosphate ion is near C1′ of the nucleoside. As the glycosidic bond breaks, the oxocarbenium intermediate is captured by the negatively charged phosphate, which is located on the other side of the ribose with respect to the purine base. This positioning of substrates guarantees inversion at C1′ during product formation. Evidence for an oxocarbenium intermediate, with bond breaking far ahead of bond making in the phosphorolysis reaction, has accumulated in the literature through kinetic isotope effect studies (*21*−*23*). However, the secondary isotope effects also suggest significant involvement of C5′, even though this is not apparent from the structural studies.

When superimposed, the free purine base is closer to Asn243, Glu201, and the active site water molecule when compared to the corresponding nucleoside (Figure 7). This observation holds irrespective of whether phosphate or ribose 1-phosphate is bound. When the ribose position of ribose 1-phosphate is compared with that of the nucleoside complex, the C1 position changes most (1.7 Å); other changes decrease in the order C2 (0.8 Å), O4 (0.7 Å), C3 (0.2 Å), and C4 (0.2 Å). The phosphate position differs slightly in the two complexes; however, all of the hydrogen bonds remain the same, even though phosphate rotates around the O1−P axis by a few degrees. This rotation moves O1 on phosphate closer to C1′ of the sugar ring (Figure 7), which provides additional evidence that O1 of phosphate is the oxygen that attacks C1′ to form ribose 1-phosphate.

The PNP−inosine−sulfate complex and the PNP−9-deazainosine−phosphate complex are good models for the enzyme−substrate complex, and the PNP−9-deazahypoxanthine−ribose 1-phosphate complex and the hypoxanthine−ribose 1-phosphate complex are good models for the PNP−product complex after phosphorolysis. The striking similarities between the structures of the PNP−substrate and the PNP−product complexes suggest that only small movements are required to generate the transition state and subsequent intermediate. A simple transition state model can be generated by averaging the positions of the two sets of atoms in the complexes (Figure 7) and then constraining the resulting structure such that (1) overall structural changes are minimized, (2) hydrogen bonds to substrates are maintained, and (3) the C1′−O4′ bond and attached atoms of the oxocarbenium ion are restrained to be planar. The transition state based on this model is shown in Figure 8. The model is consistent with the mechanism proposed by Erion et al. (*1*) but includes the details of hydrogen bonding derived from the high-resolution structures of the bovine PNP complexes.

Comparison of the PNP−substrate and PNP−product complexes provides some evidence for the molecular motions that take place during the reaction. When PNP binds phosphate, its position is fixed by the formation of a number of hydrogen bonds from main chain atoms, side chain atoms, a water molecule, and the 2′- and 3′-hydroxyl groups of the ribosyl group. One side of the bound phosphate anion is exposed and faces the nucleoside binding site, which helps

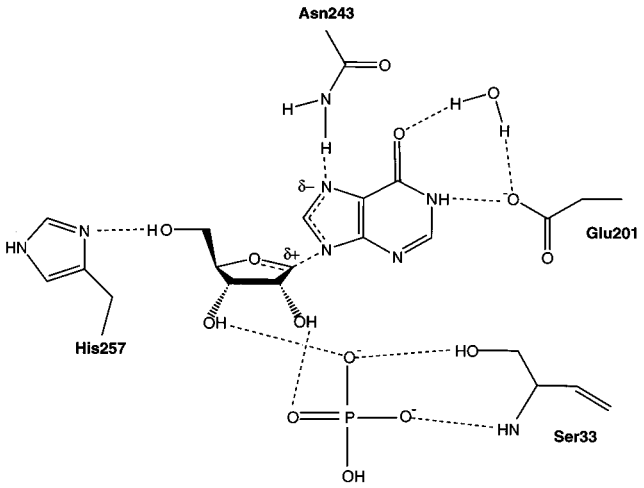

FIGURE 8: Structure of the transition state for the PNP-catalyzed reaction based on the refined structures of PNP complexes. During phosphorolysis, the proposed transition state leads to an oxocarbenium ion that is subseqeuently trapped by the negatively charged phosphate ion.

to polarize and elongate the glycosidic bond. Ser33 orients the key O1 atom on phosphate, and the 3′-hydroxyl orients the ribose with respect to phosphate O1. Asn243 and Glu201 correctly orient the purine base of the nucleoside. In addition, Asn243 provides a hydrogen bond that is essential for catalysis. The water molecule associated with Glu201 may also help to stabilize the negative charge that accumulates in the transition state by formation of a hydrogen bond to O6. As the reaction proceeds and C1′ and N9 begin to separate and move in opposite directions, the phosphate ion rotates slightly to move closer to C1′ and the ribose shifts so that C1′ and O4′ move toward O1 of the phosphate. Atoms C4′ and C5′ remain relatively fixed; however, C1′ and H1′ flip to the opposite side of the ribose ring, resulting in inversion of the configuration at C1′. As bond breaking proceeds, the purine base moves deeper into the active site and the hydrogen bond between O6 and the active site water molecule is strengthened. The phosphate and hypoxanthine remain in almost the same positions and maintain the same hydrogen bonds throughout the reaction. Consequently, the oxocarbenium ion intermediate shuttles between the leaving group and nucleophile almost entirely though the movement of C1′. Interestingly, H1′ of the intermediate would be close to the carbonyl oxygen of Ala116, which might stabilize the oxocarbenium ion through a CH···O hydrogen bond.

In summary, a series of PNP complexes have been described which provide information about the structures at various points along the catalysis pathway, including the transition state. The data show that, in addition to the conformational change induced by purine or purine nucleoside, two conformational changes, which are independent of purine or purine nucleoside binding, are caused by phosphate binding. We were unable to prepare the PNP complex with ribose 1-phosphate alone, suggesting that its affinity for PNP may be increased by purine base binding. The data provide structural details of the catalytic mechanism, and the collection of structures may be helpful in the design of new PNP inhibitors.

ACKNOWLEDGMENT

We thank Dr. John Montgomery of Southern Research Institute for providing 9-deazahypoxanthine and 7-deazainosine, Dr. Robert Klein of Montefiore Medical Center for providing 9-deazainosine, and Dr. Joel Tuttle of Burroughs Wellcome for providing acyclovir diphosphate.

REFERENCES

1. Erion, M. D., Stoeckler, J. D., Guida, W. C., Walter, R. L., and Ealick, S. E. (1997) Purine nucleoside phosphorylase. 2. Catalytic mechanism, *Biochemistry 36*, 11735−11748.
2. Parks, R. E., Jr., and Agarwal, R. B. (1972) Purine nucleoside phosphorylase, in *The Enzymes* (Boyer, P. D., Ed.) Vol. 7, pp 483−514, Academic Press, New York.
3. Giblett, E. R., Ammann, A. J., Wara, D. W., Sandman, R., and Diamond, L. K. (1975) Nucleoside-phosphorylase deficiency in a child with severely defective T-cell immunity and normal B-cell immunity, *Lancet 1*, 1010−1013.
4. Ealick, S. E., Rule, S. A., Carter, D. C., Greenhough, T. J., Babu, Y. S., Cook, W. J., Habash, J., Stoeckler, J. D., Parks, R. E., Jr., Chen, S., and Bugg, C. E. (1990) Three-dimensional structure of human erythrocytic purine nucleoside phosphorylase at 3.2 Å resolution, *J. Biol. Chem. 265*, 1812−1820.
5. Bzowska, A., Luic, M., Schroder, W., Shugar, D., Saenger, W., and Koellner, G. (1995) Calf spleen purine nucleoside phosphorylase: Purification, sequence and crystal structure of its complex with an N(7)-acycloguanosine inhibitor, *FEBS Lett. 367*, 214−218.
6. Koellner, G., Luic, M., Shugar, D., Saenger, W., and Browska, A. (1997) Crystal structure of calf spleen purine nucleoside phosphorylase in a complex with hypoxanthine at 2.15 Å resolution, *J. Mol. Biol. 265*, 202−216.
7. Ealick, S. E., Babu, Y. S., Bugg, C. E., Erion, M. D., Guida, W. C., Montgomery, J. A., and Secrist, J. A., III (1991) Application of crystallographic and modeling methods in the design of purine nucleoside phosphorylase inhibitors, *Proc. Natl. Acad. Sci. U.S.A. 88*, 11540−11544.
8. Navaza, J. (1994) AMoRe: an automated package for molecular replacement, *Acta Crystallogr. A50*, 157−163.
9. Brünger, A. T. (1988) *XPLOR Manual*, Version 3.1, Yale University Press, New Haven, CT.
10. Brünger, A. T. (1992) Free R value: a novel statistical quantity for assessing the accuracy of crystal structures, *Nature 355*, 472−475.
11. Engh, R. A., and Huber, R. (1991) Accurate bond and angle parameters for X-ray protein structure refinement, *Acta Crystallogr. A47*, 392−400.
12. Tuttle, J. V., and Kenitsky, T. A. (1984) Effects of acyclovir and its metabolites on purine nucleoside phosphorylase, *J. Biol. Chem. 259*, 4065−4069.
13. Kabsch, W. (1976) A solution for the best rotation to relate two sets of vectors, *Acta Crystallogr. A32*, 922−923.
14. Ropp, P. A., and Traut, T. W. (1991) Purine nucleoside phosphorylase. Allosteric regulation of a dissociating enzyme, *J. Biol. Chem. 266*, 7682−7687.
15. Erion, M. D., Takabayashi, K., Smith, H. B., Kessi, J., Wagner, S., Honger, S., Shames, S. L., and Ealick, S. E. (1997) Purine nucleoside phosphorylase. 1. Structure−function studies, *Biochemistry 36*, 11725−11734.
16. Noel, J. P., Hamm, H. E., and Sigler, P. B. (1993) The 2.2 Å crystal structure of transducin-α complexed with GTPγS, *Nature 366*, 654−663.
17. Lambright, D. G., Noel, J. P., Hamm, H. E., and Sigler, P. B. (1994) Structural determinants for activation of the α-subunit of a heterotrimeric G protein, *Nature 369*, 621−628.
18. Mao, C., Cook, W. J., Zhou, M., Koszalka, G. W., Krenitsky, T. A., and Ealick, S. E. (1997) The crystal structure of *Escherichia coli* purine nucleoside phosphorylase at 2.0 Å resolution, *Structure 5*, 1373−1383.
19. Kline, P. C., and Schramm, V. L. (1992) Purine nucleoside phosphorylase. Inosine hydrolysis, tight binding of the hy-

poxanthine intermediate, and third-the-sites reactivity, *Biochemistry 31*, 5964−5973.
20. Carlson, J. D., and Fischer, A. G. (1979) Thyroid purine nucleoside phosphorylase. II. Kinetic model by alternate substrate and inhibition studies, *Biochim. Biophys. Acta 566*, 259−265.
21. Stein, R. L., and Corder, E. H. (1981) Kinetic alpha-deuterium isotope effects for *Escherichia coli* purine nucleoside phsophorylase-catalyzed phosphorolysis of adenosine and inosine, *J. Biol. Chem. 256*, 767−772.
22. Lehikoinen, P. K., Sinnott, M. L., and Krenitsky, T. A. (1989) Investigation of alpha-deuterium kinetic isotope effects on the purine nucleoside phosphorylase reaction by the equilibrium-perturbation technique, *Biochem. J. 257*, 355−359.
23. Kline, P. C., and Schramm, V. L. (1993) Purine nucleoside phosphorylase. Catalytic mechanism and transition-state analysis of the arsenolysis reaction, *Biochemistry 32*, 13212−13219.
24. Carson, M. (1987) Ribbon models of macromolecules, *J. Mol. Graphics 5*, 103−106.
25. Sack, J. S. (1988) CHAIN−a crystallographic modeling program, *J. Mol. Graphics 6*, 244−245.

BI9723919